ACS OMEGA

http://pubs.acs.org/journal/acsodf

Article

Au-Based Thin-Film Metallic Glasses for Propagating Surface Plasmon Resonance-Based Sensor Applications

Cheng Wang,[†] Pin-Jie Chen,[†] and Chun-Hway Hsueh*

Cite This: *ACS Omega* 2022, 7, 18780−18785

Read Online

ACCESS | Metrics & More | Article Recommendations

ABSTRACT: We deposited Au−Cu−Si, an Au-based thin-film metallic glass (TFMG) of ∼50 nm thickness, as the activation layer for propagating surface plasmon resonance (PSPR)-based sensors on a BK7 glass substrate to substitute the commonly used gold layer. The film composition was tuned to yield the maximum Au content (∼65 at %), while the structure remained amorphous. The results showed that the Au-based TFMG could support surface plasmon resonance and gave rise to the extinction in the angle-resolved reflection spectrum. Using deionized water and ethyl alcohol with the refractive index difference of ∼0.03 as the analytes, the angle shift given by Au-based TFMG was 4° compared to 5° given by the Au film. Hence, Au-based TFMG is feasible to be used as the activation layer in PSPR-based sensors. Compared to the Au film, Au-based TFMG has the advantages of being less expensive, lacking grain boundary scattering, better adhesion to the substrate, and higher resistance to scratch and corrosion because of its amorphous structure with excellent mechanical properties.

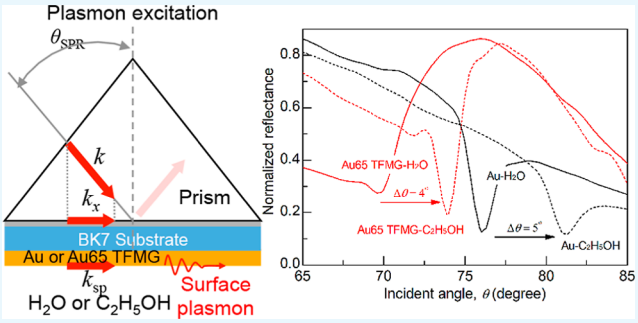

1. INTRODUCTION

Surface plasmon resonance (SPR) is a concept of nonradiative electromagnetic (EM) surface wave for macroscopic interfaces which is related to the collective oscillation of conduction electrons on the metal surface due to the excitation of the incident light at the metal−dielectric interface.[1−3] Comprehensive reviews on SPR[4,5] and its applications for optical biosensors[6−9] have been performed recently. The ordered array of metal nanoparticles resulting in high-quality factors of plasmonic surface lattice resonances has also been reviewed,[10,11] and the recent state-of-art achievements in the field of plasmonic biosensing-based terahertz spectroscopy using toroidal metadevices has been reviewed by Ahmadivand et al.[12,13] In addition, comprehensive coverage of recent design and development, including processing and fabrication, of 2D materials in the context of plasmonic-based devices has also been provided.[14] The SPR modes can be generally divided into two types, propagating surface plasmon resonance (PSPR) and localized surface plasmon resonance (LSPR).[15] PSPR, also known as surface plasmon polariton, is induced by evanescent EM waves at the planar metal−dielectric interfaces. Different from PSPR, LSPR occurs at the surface of metallic nanostructures due to the confinement of EM waves.[16−19] Both PSPR- and LSPR-based sensors can detect the change in the refractive index of the dielectric medium. Compared to the LSPR-based sensor, the PSPR-based sensor has a higher refractive index sensitivity (∼2×10^6 vs ∼2×10^2 nm RIU^{-1}) and a longer EM field decay length (200−300 vs 5−15 nm).[20] However, combining the two abovementioned factors, both the PSPR-based sensor and LSPR-based sensor are very competitive in their sensitivities.[20]

The performance of the SPR sensor can be commonly determined in two parts. On the one hand, the sensitivity is a concern and the shift of resonance angle should be large even in the case of a small change in the refractive index of the dielectric medium. On the other hand, the accuracy is the concern and the smaller full width at half maximum of the corresponding SPR spectrum represents the higher accuracy. A comprehensive list of comparisons of the performance of biosensors in terms of limit of detection and sensitivity among different optical sensing schemes could be found elsewhere.[6] For both PSPR and LSPR, plasmonic material is the basic to excite plasmons and it is required to have a negative real component and a small, positive imaginary component of the dielectric constant.[1,21−23] Thus, noble metals, such as gold and silver have been commonly used as the substrates of SPR-based sensors. Compared with silver, gold has an inert nature with higher chemical stability and direct functionalization[6]

Received: March 15, 2022
Accepted: May 19, 2022
Published: May 26, 2022

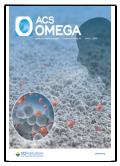

Scheme 1. Schematic Illustration of the Fabrication of Au-Based TFMGs for PSPR-Based Sensor Applications

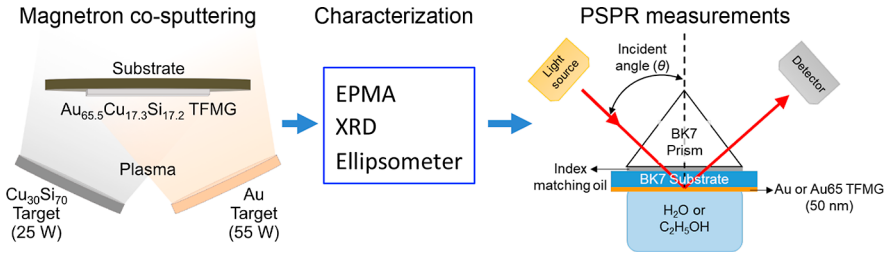

with excellent sensitivity to the change of refractive index of the dielectric medium.

Metallic glasses (MGs) are obtained by rapid quenching from the melt to the solid amorphous state.[24,25] Different from the ordered atomic arrangement of crystalline alloys, MGs have a liquid-like random atomic arrangement due to the rapid quenching process. Thus, crystalline defects, such as dislocations, grain boundaries, and voids, would not appear. Due to the absence of crystalline defects, MGs have excellent mechanical properties and have been studied extensively for engineering applications. However, the studies of the optical properties of MGs have been sparse. In the absence of grain boundaries in amorphous MGs, damping due to scattering at grain boundaries would not occur and would benefit the plasmonic applications.[26−29] Specifically, the effects of grain size of crystalline materials on surface-enhanced Raman scattering (SERS) were first studied by Dawson et al.,[26] and it was found that the SERS signals obtained from the slow-deposited Ag films with the larger grain sizes were higher than those obtained from the fast-deposited Ag films with the smaller grain sizes. Since then, the concept of elastic scattering of surface-plasmon polaritons at grain boundaries was proposed, which would result in the increasing internal damping and decreasing SERS intensity.[27,28]

Thin-film metallic glasses (TFMGs) are a new group of MGs which have been commonly fabricated by physical vapor deposition (PVD).[30−35] With the process of vapor-to-solid by PVD, TFMGs are subjected to a much faster cooling rate compared to the process of liquid-to-solid by casting for bulk MGs. As a result, TFMGs not only possess the unique properties of MGs but also have a better glass-forming ability with a wider composition range.[36,37] Moreover, TFMGs can exhibit higher fracture resistance compared with their bulk MG counterparts because of the size effect.[37,38] Previously, we have confirmed the Au-based TFMGs as a plasmonic material, used nanoimprint to fabricate periodic nanostructures by taking advantage of the viscous flow behavior of TFMGs in the supercooled liquid region, and proved the feasibility of using Au-based TFMGs as LSPR-based sensor.[39] In addition, we have studied the effects of crystallinity of Au-based TFMGs on SERS recently.[29] Specifically, the as-deposited Au-based TFMGs were imprinted in the supercooled liquid region to develop the periodic nanostructures. The imprinted amorphous films were then heat-treated at different temperatures to obtain different crystallinities. Using crystal violet as the analyte, the Raman spectra were measured and the intensity showed an initial quick decrease and then a slow increase with the increasing heat treatment temperature. In this case, the Raman intensity decreased upon the initial crystallization of heat-treated amorphous film due to scattering at grain boundaries, and the grain growth at higher heat-treated temperatures resulted in the reduction of grain boundary area and the Raman intensity increased.[29] In the present study, we utilized the Au-based TFMGs as the activation layer in the PSPR-based sensor to substitute the traditional gold layer to reduce the cost. Also, compared to pure Au, the absence of crystalline defects and better adhesion to the substrate would result in the absence of grain boundary scattering and excellent scratch/corrosion resistance of Au-based TFMGs.

2. EXPERIMENTAL PROCEDURE

The schematic illustration of the fabrication process of Au-based TFMGs for PSPR-based sensor applications is shown in Scheme 1.

2.1. Sputtering. The Au-based TFMGs were deposited on BK7 glass substrates by magnetron co-sputtering from an Au target and a $Cu_{30}Si_{70}$ target. While both Au and Cu are plasmonic materials, Si with a small atomic size was added to facilitate the formation of an amorphous structure. The purities of both targets were over 99.99 wt %, and the distance between the substrate and the target was fixed at 10 cm. The background pressure of the system was lower than 5×10^{-5} Pa, and the working pressure was maintained by Ar gas at 0.3 Pa. While the radio frequency power (13.56 MHz) was set at 55 W for the Au target, the direct current power was set at 25 W for the $Cu_{30}Si_{70}$ target. To keep the uniform distribution of elements in the film, the substrate holder with a diameter of 10.16 cm was rotated at a speed of 60 rpm. It is worth noting that the effects of Ar working pressure, ranging from 0.4 to 10 Pa, on the growth mode of Au-based TFMGs were studied by Denis et al.,[34] and the surface morphology changed from homogeneous at low working pressures to nanostructured morphology at high working pressures.

2.2. Characterization. To measure the compositions of Au-based TFMG, an electron probe X-ray microanalyzer (EPMA, JEOL, JXA-8200) with an accelerating voltage of 10 kV and an electron beam size of 10 μm was used, and the data were collected randomly from seven points. The structure of the sample was investigated by X-ray diffraction (XRD, Rigaku, TTRAX 3) using Cu-Kα radiation (λ = 0.14506 nm) with a grazing incident angle of 0.7° and 2θ scanned from 20 to 60° at a scanning rate of 4°/min. The real part, ε_r, and the imaginary part, ε_i, of the dielectric constants and the reflectance were measured by a spectroscopic ellipsometer (J.A. Woolam Co, M-2000 Ellipsometer) to check the feasibility of Au-based TFMG as PSPR-based activation layer and to investigate the angle shift of PSPR when different dielectric media were used as analytes.

The different dielectric properties and crystallinities with the different contents of Au in Au-based films were systematically studied in our previous works.[39,40] As the content of Au increased in the Au-based film, the dielectric constant would become closer to that of Au.[39] However, the degree of crystallinity would simultaneously increase with the increasing

https://doi.org/10.1021/acsomega.2c01565
ACS Omega 2022, 7, 18780−18785

Au content in the Au-based film, and the maximum Au content could be achieved with the amorphous structure was ~65 at %.[40] In this study, the compositions were measured by EPMA and the sample was named by the atomic percentage of Au in the film. To obtain the maximum Au content and simultaneously control the structure in the amorphous state, Au65 TFMG, for which Au, Cu, and Si contents were 65.5 ± 0.2, 17.3 ± 0.2, and 17.2 ± 0.1 at %, respectively, was chosen as the activation layer in the PSPR-based sensor.

2.3. PSPR Measurements. The selection of material for the glass prism used in PSPR measurements has been discussed by Singh et al.[41] and it is usually based on the resonance wavelength. Specifically, BK7, SF2, and SF10 have been selected for visible light-PSPR; sapphire and quartz prisms are used for UV−PSPR; and fluoride glass prism is suitable for NIR−PSPR. Because the resonance wavelength in our work was in the range of visible light, BK7 glass was selected for the present study. Specifically, the BK7 glass prism purchased from Precision Systems Industrial Ltd. with a width of 20 mm was used in the present study. The surface of the prism in contact with the substrate was fully covered by the substrate during the PSPR measurements. Prior to each PSPR measurement, the sensor surface was cleaned by rinsing in acetone, alcohol, and deionized water each for at least 1 min in sequence and then heat-dried to remove the residual liquid. A comparative analysis of using different prisms was not performed in the present study. However, it is worth noting that the effects of using different prisms (SiO_2, BaF_2, CsF, and BK7), different plasmonic metals (Au, Ag, Cu, and Al), and doping in the intermediate layer on the sensitivity improvement of the PSPR sensor was investigated recently by Kumar et al.[42]

3. RESULTS AND DISCUSSION

3.1. Structure. The surface morphologies of Au-based TFMGs scanned by the Berkovich nanoindenter with a scanned area of 20 μm × 20 μm at various temperatures were obtained in our previous work.[40] The surface of the as-deposited film was homogeneous and smooth at room temperature, which agreed with Denis et al.'s results of sputtering at low working pressures,[34] and became rough and granular when the temperature reached the crystallization temperature.[40] The cross-sectional SEM image of Au65 TFMG deposited on the BK7 glass substrate is shown in Figure 1, and the thickness of Au65 TFMG was about 50 nm.

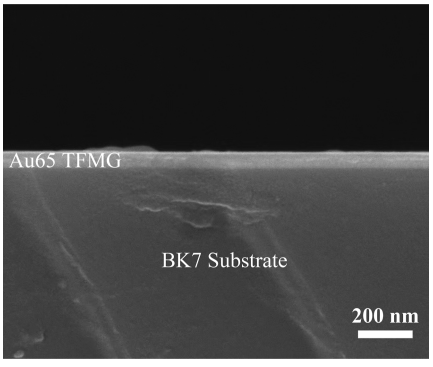

Figure 1. SEM image showing the cross-section of Au65 TFMG on the BK7 glass substrate.

The XRD spectra of Au and Au65 TFMG are shown in Figure 2. The spectrum for Au showed the crystalline peaks at

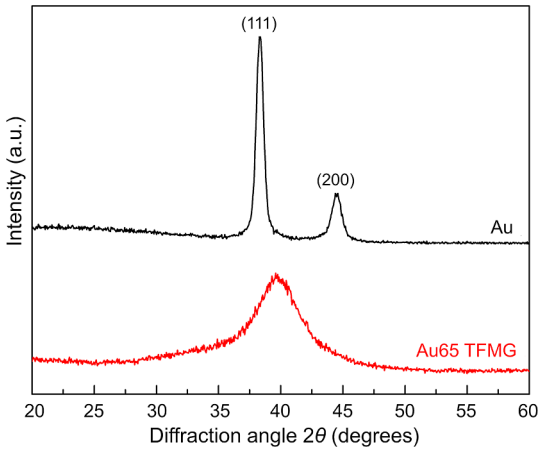

Figure 2. XRD spectra of Au and Au65 TFMG (scanning rate of 4°/min).

38.2 and 44.4° in 2θ and were identified to be that of the (111) and (200) lattice planes, respectively, of the face-centered cubic Au structure (JCPDS 04-0784). For Au65 TFMG, the broad peak around 40.5° and a lack of crystalline peaks supported the amorphous structure of the film. Upon annealing of Au65 TFMG at 200 °C for 10 min, a sharp crystalline peak appeared at 40.5° (not shown), which could be identified as the (400) lattice plane of simple cubic AuCu (JCPDS 38-0741).

3.2. Dielectric Properties. The dielectric constants of Au65 TFMG were measured by an ellipsometer in the wavelength range of 370−1200 nm, and the results are shown in Figure 3. For comparison, the dielectric constants of pure Au and Pt (data taken from Palik's handbook) are also included in Figure 3. The value of ε_r of Au65 TFMG was similar to that of pure Au in the visible light range (400−700 nm), as shown in Figure 3a. The value of ε_i of Au65 TFMG, shown in Figure 3b, was higher than that of pure Au representing the higher energy loss and lower sensitivity; however, it was sufficiently low in the visible light range. Specifically, it was lower than Pt, one of the plasmonic materials. Hence, the dielectric constants shown in Figure 3 supported the feasibility of Au65 TFMG as a plasmonic material in the visible light range. However, it was not suitable to be used in the infrared region for the wavelength modulation spectroscopy.

3.3. PSPR Measurements. The instrument set-up for PSPR measurements is schematically shown in Figure 4. The Au film and Au65 TFMG with a thickness of ~50 nm, which has been commonly adopted in PSPR measurements, were deposited, respectively, on a BK7 (refractive index n = 1.5168) glass substrate. While the uniform and continuous films could not be achieved for the thinner films, too much adsorption would occur for the thicker films. The PSPR substrate was attached to a BK7 prism with index-matching oil (n = 1.5150 ± 0.0002) to eliminate the reflection/refraction losses associated with the interface and to keep intimate contact between the BK7 prism and BK7 substrate in order to avoid the air gap in between. Deionized water (H_2O with polar covalent hydrogen-oxygen bonds) and ethyl alcohol (CH_3-CH_2-OH with nonpolar covalent carbon-hydrogen bonds and polar covalent

https://doi.org/10.1021/acsomega.2c01565
ACS Omega 2022, 7, 18780−18785

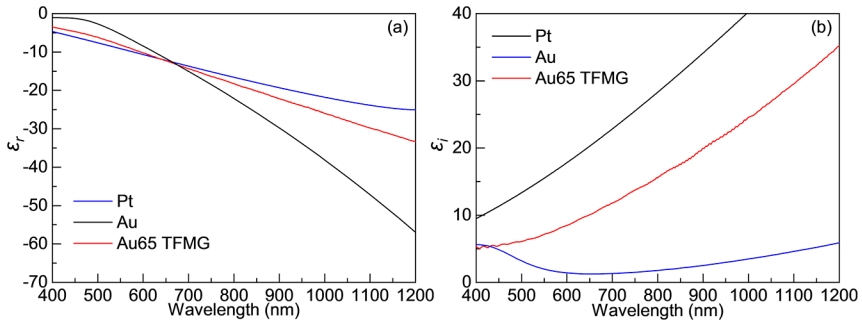

Figure 3. (a) Real part, ε_r, and (b) imaginary part, ε_i, of the dielectric constants of Au65 TFMG and pure Au film measured by an ellipsometer. The data for Pt were taken from Palik's handbook.

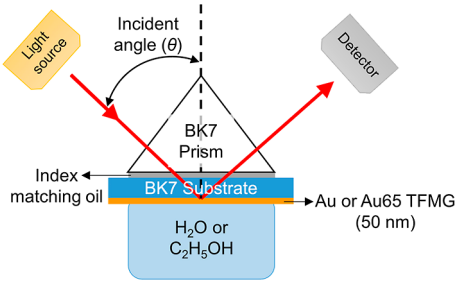

Figure 4. Schematic diagram of instrument set-up for angle-resolved PSPR-based sensors.

carbon-oxygen and hydrogen-oxygen bonds) with refractive indexes of 1.333 and 1.361, respectively, were used as analytes in the PSPR measurements. Polarized incident light with its wavelength in the range of 370 to 1690 nm was illuminated through the prism onto the film to select the most efficient wavelength for conducting PSPR measurements. The prism, film, and container were fixed on the stage, and the reflectance was measured by a spectroscopic ellipsometer with an angle of incidence ranging from 65 to 85°.

The phenomenon of PSPR is schematically shown in Figure 5. When the incident angle reaches a critical value (θ_{SPR}), the condition of resonance is fulfilled and a sharp dip of optical reflectance would appear. This resonance angle (θ_{SPR}) depends on the refractive index of the dielectric medium, and the change of refractive index near the metal/dielectric interface would result in a shift of θ_{SPR}; that is, $\Delta\theta_{SPR}$, to be detected.[43] Thus, PSPR can be used to detect the change of refractive index at the interface and further be applied as high sensitivity sensor in the field of optics.[1,44,45]

Using deionized water and ethyl alcohol as the analytes in the PSPR measurements, the reflectance intensity versus incident angle curves are shown in Figure 6 (in which each

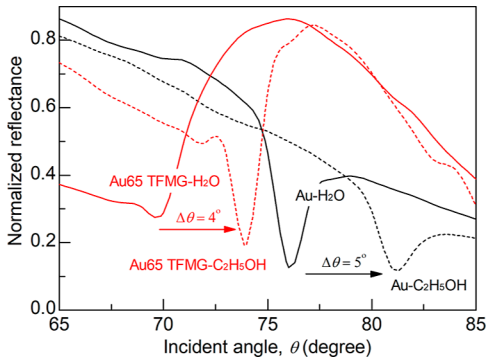

Figure 6. Resonance angles (θ_{SPR}) for deionized water and ethyl alcohol with a small refractive index difference of ~0.03 were measured to verify that Au65 TFMG is a potential candidate for PSPR-based sensors.

curve is the average of 50 measurements) for Au film and Au65 TFMG, respectively, as the activation layers. With a difference in the refractive index of ~0.03 between deionized water and ethyl alcohol and an incident wavelength of 850 nm, the angle shifts, $\Delta\theta_{SPR}$, for Au thin film and Au65 TFMG were 5 and 4°, respectively, when the analyte was switched from deionized water to ethyl alcohol. Therefore, the Au65 TFMG could be regarded as a potential candidate for PSPR-based sensors. In addition, while the gold layer was prone to damage and detachment after repeated usage and cleaning, the Au-based TFMG showed good reusability because of the improved

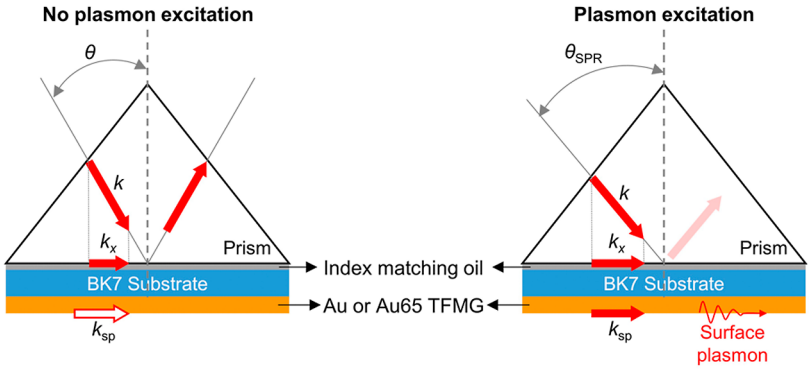

Figure 5. Schematic diagrams showing no plasmon excitation and plasmon excitation phenomena of PSPR.

https://doi.org/10.1021/acsomega.2c01565
ACS Omega 2022, 7, 18780−18785

adhesion to the substrate. Also, because of the amorphous nature, the Au-based TFMG has excellent corrosion resistance and could be applied to a wider range of analytes compared to the gold layer. However, the service life of Au-based TFMG was not studied in the present work, and we hope to study the durability issue in the future. Also, while deionized water and ethyl alcohol with a refractive index difference of ∼0.03 were used as the analytes in the present work, it would be more meaningful if Au-based TFMG could be used for more practical testing (such as biomass testing), and we hope to perform this study in the future work. It is worth noting that the prism structure was used in the present study for sensing. This structure has a number of disadvantages, including a bulky structure and moving components. On the other hand, fiber structure has been developed recently[6] and it has the advantages of low EM interference, small sizes, multiplexing, and remote sensing capabilities, and it could be preferable over the prism structure.[6]

4. CONCLUSIONS

In conclusion, the feasibility of using the amorphous Au65 TFMG fabricated by magnetron co-sputtering as the activation layer in the PSPR-based sensor was verified in the present study. Compared to the traditional activation layer of Au film, Au65 TFMG had slightly inferior dielectric properties (Figure 3) to be used as the plasmonic material because of the lower gold content in the film. As a result, the sensitivity of Au65 TFMG as a PSPR-based sensor was slightly lower than that of the Au film. Nevertheless, using water (n = 1.333) and ethyl alcohol (n = 1.361) with the refractive index difference of ∼0.03 as the analytes, the angle shift given by Au film was 5°, while it was only one degree less for Au65 TFMG (Figure 6). However, compared to Au film, Au65 TFMG had the advantages of being less expensive, lacking grain boundary scattering, better adhesion to the substrate, and higher resistance to scratch and corrosion[30] because of its amorphous structure. The characteristics of high scratch and corrosion resistances of Au65 TFMG made it suitable for tip-enhanced Raman scattering (TERS) applications, while the traditional TERS tips of Au and Ag had an extremely short lifetime because of low hardness and poor adhesion.[46] Our work is hoped to trigger more advanced studies on Au-based TFMGs for the potential applications of sensors.

AUTHOR INFORMATION

Corresponding Author

Chun-Hway Hsueh − *Department of Materials Science and Engineering, National Taiwan University, Taipei 10617, Taiwan;* orcid.org/0000-0002-6477-7148; Email: hsuehc@ntu.edu.tw

Authors

Cheng Wang − *Department of Materials Science and Engineering, National Taiwan University, Taipei 10617, Taiwan*

Pin-Jie Chen − *Department of Materials Science and Engineering, National Taiwan University, Taipei 10617, Taiwan*

Complete contact information is available at: https://pubs.acs.org/10.1021/acsomega.2c01565

Author Contributions

†C.W. and P.J.C. contributed equally to this study.

Notes

The authors declare no competing financial interest.

ACKNOWLEDGMENTS

This work was supported by the Ministry of Science and Technology, Taiwan under contract no. MOST 110-2221-E-002-038.

REFERENCES

(1) Willets, K. A.; Van Duyne, R. P. Localized surface plasmon resonance spectroscopy and sensing. *Annu. Rev. Phys. Chem.* **2007**, *58*, 267−297.

(2) Chen, Y.; Ming, H. Review of surface plasmon resonance and localized surface plasmon resonance sensor. *Photonic Sens.* **2012**, *2*, 37−49.

(3) Suherman, S.; Motahar Hossain, M.; Morita, K.; Kawaguchi, T. Effect of metal film, thickness and various solvents on the SPR biosensor sensitivity for illegal compound detection. *Orient. J. Chem.* **2018**, *34*, 1355−1361.

(4) Wang, Q.; Ren, Z.-H.; Zhao, W.-M.; Wang, L.; Yan, X.; Zhu, A.-S.; Qiu, F.-M.; Zhang, K.-K. Research advances on surface plasmon resonance biosensors. *Nanoscale* **2022**, *14*, 564−591.

(5) Andersson, J.; Svirelis, J.; Ferrand-Drake del Castillo, G.; Sannomiya, T.; Dahlin, A. Surface plasmon resonance sensing with thin films of palladium and platinum - quantitative and real-time analysis. *Phys. Chem. Chem. Phys.* **2022**, *24*, 4588−4594.

(6) Kaur, B.; Kumar, S.; Kaushik, B. K. Recent advancements in optical biosensors for cancer detection. *Biosens. Bioelectron.* **2022**, *197*, 113805.

(7) Kaur, B.; Kumar, S.; Kaushik, B. K. 2D Materials-based fiber optic SPR biosensor for cancer detection at 1550 nm. *IEEE Sens. J.* **2021**, *21*, 23957−23964.

(8) Li, M.; Singh, R.; Marques, C.; Zhang, B.; Kumar, S. 2D material assisted SMF-MCF-MMF-SMF based LSPR sensor for creatinine detection. *Opt. Express* **2021**, *29*, 38150−38167.

(9) Wang, Z.; Singh, R.; Marques, C.; Jha, R.; Zhang, B.; Kumar, S. Taper-in-taper fiber structure-based LSPR sensor for alanine amino-transferase detection. *Opt. Express* **2021**, *29*, 43793−43810.

(10) Kravets, V. G.; Kabashin, A. V.; Barnes, W. L.; Grigorenko, A. N. Plasmonic surface lattice resonances: a review of properties and applications. *Chem. Rev.* **2018**, *118*, 5912−5951.

(11) Wang, B.; Yu, P.; Wang, W.; Zhang, X.; Kuo, H. C.; Xu, H.; Wang, Z. M. High-Q Plasmonic Resonances: Fundamentals and Applications. *Adv. Opt. Mater.* **2021**, *9*, 2001520.

(12) Ahmadivand, A.; Gerislioglu, B.; Manickam, P.; Kaushik, A.; Bhansali, S.; Nair, M.; Pala, N. Rapid detection of infectious envelope proteins by magnetoplasmonic toroidal metasensors. *ACS Sens.* **2017**, *2*, 1359−1368.

(13) Ahmadivand, A.; Gerislioglu, B.; Ahuja, R.; Kumar Mishra, Y. Terahertz plasmonics: The rise of toroidal metadevices towards immunobiosensings. *Mater. Today* **2020**, *32*, 108−130.

(14) Raghuwanshi, S. K.; Kumar, S.; Singh, Y. *2D materials for surface plasmon resonance-based sensors*; CRC Press LLC, 2022.

(15) Jatschka, J.; Dathe, A.; Csáki, A.; Fritzsche, W.; Stranik, O. Propagating and localized surface plasmon resonance sensing - A critical comparison based on measurements and theory. *Sens. Bio-Sens. Res.* **2016**, *7*, 62−70.

(16) Hatab, N. A.; Hsueh, C.-H.; Gaddis, A. L.; Retterer, S. T.; Li, J.-H.; Eres, G.; Zhang, Z.; Gu, B. Free-standing optical gold bowtie nanoantenna with variable gap size for enhanced Raman spectroscopy. *Nano Lett.* **2010**, *10*, 4952−4955.

(17) Wi, J.-S.; Tominaka, S.; Uosaki, K.; Nagao, T. Porous gold nanodisks with multiple internal hot spots. *Phys. Chem. Chem. Phys.* **2012**, *14*, 9131−9136.

(18) Galvan, D. D.; Špačková, B.; Slabý, J.; Sun, F.; Ho, Y.-H.; Homola, J.; Yu, Q. Surface-enhanced Raman scattering on gold nanohole arrays in symmetrical dielectric environments exhibiting electric field extension. *J. Phys. Chem. C* **2016**, *120*, 25519−25529.

(19) Soualmia, F.; Touhar, S. A.; Guo, L.; Xu, Q.; Garland, M. V.; Percot, A.; El Amri, C.; El Amri, C. Amino-methyl coumarin as a potential SERS@Ag probe for the evaluation of protease activity and inhibition. *J. Raman Spectrosc.* **2017**, *48*, 82−88.
(20) Haes, A. J.; Van Duyne, R. P. A unified view of propagating and localized surface plasmon resonance biosensors. *Anal. Bioanal. Chem.* **2004**, *379*, 920−930.
(21) Li, T.; Wu, K.; Rindzevicius, T.; Wang, Z.; Schulte, L.; Schmidt, M. S.; Boisen, A.; Ndoni, S. Wafer-scale nanopillars derived from block copolymer lithography for surface-enhanced Raman spectroscopy. *ACS Appl. Mater. Interfaces* **2016**, *8*, 15668−15675.
(22) Sharma, B.; Frontiera, R. R.; Henry, A. I.; Ringe, E.; Van Duyne, R. P. SERS: Materials, applications, and the future. *Mater. Today* **2012**, *15*, 16−25.
(23) Le Thi Ngoc, L.; Yuan, T.; Oonishi, N.; van Nieuwkasteele, J.; van den Berg, A.; Permentier, H.; Bischoff, R.; Carlen, E. T. Suppression of surface-enhanced Raman scattering on gold nanostructures by metal adhesion layers. *J. Phys. Chem. C* **2016**, *120*, 18756−18762.
(24) Klement, W.; Willens, R. H.; Duwez, P. Non-crystalline structure in solidified gold-silicon alloys. *Nature* **1960**, *187*, 869−870.
(25) Yue, X.; Inoue, A.; Liu, C.-T.; Fan, C. The development of structure model in metallic glasses. *J. Mater. Res.* **2017**, *20*, 326−338.
(26) Dawson, P.; Alexander, K. B.; Thompson, J. R.; Haas, J. W., 3rd; Ferrell, T. L. Influence of metal grain size on surface-enhanced Raman scattering. *Phys. Rev. B* **1991**, *44*, 6372−6381.
(27) Yang, L.; Qin, X.; Jiang, X.; Gong, M.; Yin, D.; Zhang, Y.; Zhao, B. SERS investigation of ciprofloxacin drug molecules on TiO_2 nanoparticles. *Phys. Chem. Chem. Phys.* **2015**, *17*, 17809−17815.
(28) Shen, Y.; Miao, P.; Hu, C.; Wu, J.; Gao, M.; Xu, P. SERS-based plasmon-driven reaction and molecule detection on a single Ag@MoS_2 microsphere: Effect of thickness and crystallinity of MoS_2. *ChemCatChem* **2018**, *10*, 3520−3525.
(29) Chen, P.-J.; Hsueh, C.-H. Imprintable Au-based thin-film metallic glasses with different crystallinities for surface-enhanced Raman scattering. *J. Phys. Chem. C* **2021**, *125*, 23983−23990.
(30) Chiang, C. L.; Chu, J. P.; Liu, F. X.; Liaw, P. K.; Buchanan, R. A. A 200nm thick glass-forming metallic film for fatigue-property enhancements. *Appl. Phys. Lett.* **2006**, *88*, 131902−131905.
(31) Ketov, S. V.; Joksimovic, R.; Xie, G.; Trifonov, A.; Kurihara, K.; Louzguine-Luzgin, D. V. Formation of nanostructured metallic glass thin films upon sputtering. *Heliyon* **2017**, *3*, e00228−e00243.
(32) Etiemble, A.; Der Loughian, C.; Apreutesei, M.; Langlois, C.; Cardinal, S.; Pelletier, J. M.; Pierson, J.-F.; Steyer, P. Innovative Zr-Cu-Ag thin film metallic glass deposed by magnetron PVD sputtering for antibacterial applications. *J. Alloys Compd.* **2017**, *707*, 155−161.
(33) Liu, F. X.; Gao, Y. F.; Liaw, P. K. Rate-dependent deformation behavior of Zr-based metallic-glass coatings examined by nanoindentation. *Metall. Mater. Trans. A* **2008**, *39*, 1862−1867.
(34) Denis, P.; Liu, S. Y.; Fecht, H.-J. Growth mode transition in Au-based thin film metallic glasses. *Thin Solid Films* **2018**, *665*, 29−35.
(35) Wang, C.-W.; Yiu, P.; Shek, C.-H.; Hsueh, C.-H. Zr-Ti-Ni thin film metallic glass as a diffusion barrier between copper and silicon. *J. Mater. Sci.* **2015**, *50*, 2085−2092.
(36) Diyatmika, W.; Chu, J. P.; Kacha, B. T.; Yu, C.-C.; Lee, C.-M. Thin film metallic glasses in optoelectronic, magnetic, and electronic applications: A recent update. *Curr. Opin. Solid State Mater. Sci.* **2015**, *19*, 95−106.
(37) Chu, J. P.; Jang, J. S. C.; Huang, J. C.; Chou, H. S.; Yang, Y.; Ye, J. C.; Wang, Y. C.; Lee, J. W.; Liu, F. X.; Liaw, P. K.; Chen, Y. C.; Lee, C. M.; Li, C. L.; Rullyani, C. Thin film metallic glasses: Unique properties and potential applications. *Thin Solid Films* **2012**, *520*, 5097−5122.
(38) Glushko, O.; Mühlbacher, M.; Gammer, C.; Cordill, M. J.; Mitterer, C.; Eckert, J. Exceptional fracture resistance of ultrathin metallic glass films due to an intrinsic size effect. *Sci. Rep.* **2019**, *9*, 8281.
(39) Wang, C.; Nien, L.-W.; Ho, H.-C.; Lai, Y.-C.; Hsueh, C.-H. Surface plasmon excited on imprintable thin-film metallic glasses for surface-enhanced Raman scattering applications. *ACS Appl. Nano Mater.* **2018**, *1*, 908−914.
(40) Wang, C.; Liao, Y.-C.; Chu, J. P.; Hsueh, C.-H. Viscous flow and viscosity measurement of low-temperature imprintable AuCuSi thin film metallic glasses investigated by nanoindentation creep. *Mater. Des.* **2017**, *123*, 112−119.
(41) Singh, S.; Singh, P. K.; Umar, A.; Lohia, P.; Albargi, H.; Castañeda, L.; Dwivedi, D. K. 2D nanomaterial-based surface plasmon resonance sensors for biosensing applications. *Micromachines* **2020**, *11*, 779.
(42) Kumar, R.; Pal, S.; Prajapati, Y. K.; Kumar, S.; Saini, J. P. Sensitivity improvement of a MXene- immobilized SPR sensor with Ga-doped-ZnO for biomolecules detection. *IEEE Sens. J.* **2022**, *22*, 6536−6543.
(43) Sharma, A. K.; Jha, R.; Pattanaik, H. S. Design considerations for surface plasmon resonance based detection of human blood group in near infrared. *J. Appl. Phys.* **2010**, *107*, 034701.
(44) Petryayeva, E.; Krull, U. J. Localized surface plasmon resonance: Nanostructures, bioassays and biosensing-A review. *Anal. Chim. Acta* **2011**, *706*, 8−24.
(45) González-Díaz, J. B.; García-Martín, A.; García-Martín, J. M.; Cebollada, A.; Armelles, G.; Sepúlveda, B.; Alaverdyan, Y.; Käll, M. Plasmonic Au/Co/Au nanosandwiches with enhanced magneto-optical activity. *Small* **2008**, *4*, 202−205.
(46) Wang, C. Au-based thin film metallic glasses for plasmonic sensor applications. Ph.D. Thesis; Institute of Materials Science and Engineering, National Taiwan University, 2018.

https://doi.org/10.1021/acsomega.2c01565
ACS Omega 2022, 7, 18780−18785